Shear-Induced beta-Crystallite Unfolding in Condensed Phase Nanodroplets Promotes Fiber Formation in a Biological Adhesive

Baer, Alexander; Horbelt, Nils; Nijemeisland, Marlies; Garcia, Santiago J.; Fratzl, Peter; Schmidt, Stephan; Mayer, Georg; Harrington, Matthew J.

DOI
10.1021/acsnano.9b00857

Publication date
2019

Document Version
Final published version

Published in
ACS Nano

Citation (APA)
Baer, A., Horbelt, N., Nijemeisland, M., Garcia, S. J., Fratzl, P., Schmidt, S., Mayer, G., & Harrington, M. J. (2019). Shear-Induced beta-Crystallite Unfolding in Condensed Phase Nanodroplets Promotes Fiber Formation in a Biological Adhesive. *ACS Nano*, *13*(5), 4992-5001. https://doi.org/10.1021/acsnano.9b00857

ACS NANO

Cite This: ACS Nano 2019, 13, 4992−5001

www.acsnano.org

ARTICLE

Shear-Induced β-Crystallite Unfolding in Condensed Phase Nanodroplets Promotes Fiber Formation in a Biological Adhesive

Alexander Baer,[†] Nils Horbelt,[‡] Marlies Nijemeisland,[§] Santiago J. Garcia,[§] Peter Fratzl,[‡] Stephan Schmidt,[∥] Georg Mayer,[†] and Matthew J. Harrington*[,‡,⊥]

[†]Department of Zoology, Institute of Biology, University of Kassel, Heinrich-Plett-Str. 40, D-34132 Kassel, Germany

[‡]Department of Biomaterials, Max Planck Institute of Colloids and Interfaces, Research Campus Golm, D-14424 Potsdam, Germany

[§]Novel Aerospace Materials group, Faculty of Aerospace Engineering, Delft University of Technology, Kluyverweg 1, 2629 HS Delft, The Netherlands

[∥]Preparative Polymer Chemistry, Heinrich-Heine-Universität, Universitätsstraße 1, D-40225 Düsseldorf, Germany

[⊥]Department of Chemistry, McGill University, 801 Sherbrooke Street West, Montreal, Quebec H3A 0B8, Canada

ABSTRACT: **Natural materials provide an increasingly important role model for the development and processing of next-generation polymers. The velvet worm *Euperipatoides rowelli* hunts using a projectile, mechanoresponsive adhesive slime that rapidly and reversibly transitions into stiff glassy polymer fibers following shearing and drying. However, the molecular mechanism underlying this mechanoresponsive behavior is still unclear. Previous work showed the slime to be an emulsion of nanoscale charge-stabilized condensed droplets comprised primarily of large phosphorylated proteins, which under mechanical shear coalesce and self-organize into nano- and microfibrils that can be drawn into macroscopic fibers. Here, we utilize wide-angle X-ray diffraction and vibrational spectroscopy coupled with *in situ* shear deformation to explore the contribution of protein conformation and mechanical forces to the fiber formation process. Although previously believed to be unstructured, our findings indicate that the main phosphorylated protein component possesses a significant β-crystalline structure in the storage phase and that shear-induced partial unfolding of the protein is a key first step in the rapid self-organization of nanodroplets into fibers. The insights gained here have relevance for sustainable production of advanced polymeric materials.**

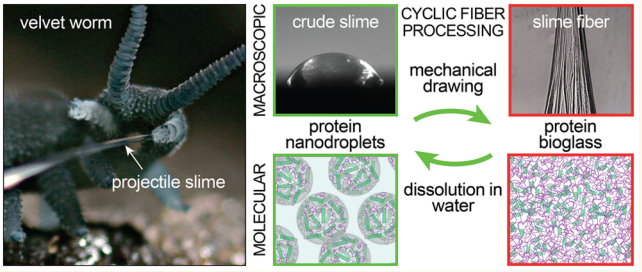

KEYWORDS: *self-assembly, coacervate, bioinspiration, nanodroplets, mechanoresponsive, Onychophora*

Protein-based biopolymeric fibers, such as silk and mussel byssus, are important archetypes for the bioinspired design of new polymeric materials with advanced properties (*e.g.*, self-healing, wet adhesion, exceptional toughness).[1−3] Aside from mechanical performance, possibly the most enviable and elusive property of these materials from the perspective of biomimicry and material fabrication is the ease and economy of processing as the fluid precursors transition into a solid. Indeed, in these systems, a concentrated fluid protein dope rapidly transforms into a high-performance fiber under ambient conditions without the need for harsh solvents or high temperatures and without producing toxic byproducts. Elucidation of the underlying physical and chemical mechanisms driving supramolecular self-assembly of proteins into natural materials is required to understand the origin of their outstanding properties, as evidenced by recent successes in artificial silk spinning.[2] In this regard, the adhesive fibers from onychophorans, which form outside the body of the organism (Figures 1A−D), present a fascinating model system for understanding environmentally friendly processing of recyclable polymeric materials.[4,5]

Onychophorans, known commonly as velvet worms, are terrestrial invertebrates inhabiting the forest floors of subtropical and equatorial regions, which utilize a sticky fluid slime for prey capture and defense that is discharged from specialized limbs on the head, known as slime papillae (Figure 1A).[6,7] After deployment, the slime transitions in midair into gel-like threads that rapidly dry to form glassy polymeric fibers with high stiffness.[5] Velvet worm slime is thus a mechanoresponsive protein solution, which is stored in reservoirs of large slime glands within the organism until ejection during

Received: January 30, 2019
Accepted: April 1, 2019
Published: April 1, 2019

DOI: 10.1021/acsnano.9b00857
ACS Nano 2019, 13, 4992−5001

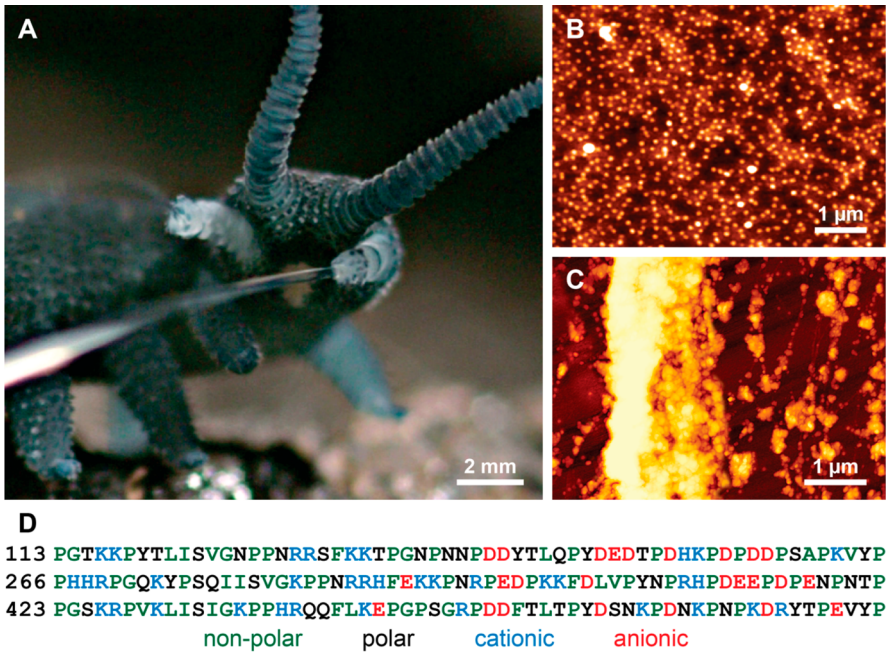

Figure 1. Fiber formation from velvet worm slime. (A) Onychophorans utilize a projectile capture slime for hunting and defense, which rapidly transitions from a sticky fluid to glassy fibers. (B) The slime is an emulsion of monodisperse nanoscale droplets that (C) aggregate and form nano- and microfibrils following mechanical agitation. (D) A small portion of the sequence of the dominant protein making up the slime and fibers of *Euperipatoides rowelli*, known as Er_P1 (Genbank accession number: HM217027), showing a repetitive region with alternating patches of positively and negatively charged amino acids and high proline content.[12]

hunting.[8−10] In the liquid state, the proteins remain in an essentially inactive form; however, mechanical agitation of the slime appears to cause the component proteins to rapidly transition from their dormant storage state into a stiff fiber state *via* a combination of shear forces and evaporation.[5] However, unlike arachnid and insect silks,[11] the transition from fluid dope to stiff fibers can be induced *ex vivo* by simple mechanical shearing and drawing of the extracted dope solution.[5] Previous studies have identified the primary biomolecular component as a large (∼300 kDa) proline-rich zwitterionic protein (Figure 1D), which is believed to be highly phosphorylated.[4,10,12] Recent findings revealed the slime from several species to be nanoemulsions of monodisperse spherical droplets (Ø ∼ 70 nm) comprised primarily of proline-rich proteins and a minor lipid content, which are charge stabilized into a dense fluid-like phase, possibly as an internal or complex coacervate (Figure 1B).[4,5,13] Notably, worm slime fibers are resoluble with extended exposure to water, resulting in reformation of monodisperse nanodroplets, which can be further formed into regenerated fibers upon reapplication of mechanical shearing.[5] This indicates that the "instructions" for circular fiber assembly are encoded in the mechanoresponsive droplets themselves, likely within the primary and higher order structure of the biomolecules that comprise it.

Previous reports suggest that the proteins in the slime fibers of the Australian velvet worm species *Euperipatoides rowelli*[14] are unstructured based on their high proline content (a known helix breaker; Figure 1D);[12] however, investigations of the slime of other species suggest the presence of regular secondary structures in the component proteins, including *β*-sheet structure.[13,15] Here, we undertake a multiscale experimental investigation utilizing X-ray diffraction and vibrational spectroscopy with *in situ* shear deformation to characterize the protein conformation within *E. rowelli* slime and fibers to determine how structure and organization change as a function of mechanoresponsive fiber self-assembly. Our results reveal that slime proteins possess a high content of *β*-crystalline structure in the storage phase, which is partially lost during fiber formation upon shear stress. These findings reveal important insights into the physical and biochemical principles underlying this reversible process, which could prove highly relevant for inspiring production of next-generation recyclable polymers and plastics.

RESULTS AND DISCUSSION

Wide-angle X-ray Diffraction (WAXD) of Slime and Fibers Indicates *β*-Crystalline Structure. Previously, WAXD studies were performed only on dried velvet worm slime fibers of *E. rowelli* and were unable to detect a diffraction pattern or even a diffuse scattering signal, leading the authors to propose a non-ordered protein structure.[12] However, studies of slime from other onychophoran species indicate a secondary structure based on spectroscopic investigations.[13,15] In order to investigate the possibility of regular protein conformation in the slime, we performed WAXD on three different samples: (i) dried crude slime, (ii) thick droplets formed on the coating of drawn fibers; and (iii) washed fibers (core only) in which the coating was removed (Figure 2A). As an X-ray source, high-brilliance synchrotron radiation was utilized to probe protein conformation with enhanced sensitivity. Dried crude slime and fiber droplets gave a strong and very similar diffraction pattern consisting of two broad concentric rings (Figure 2A). As previously reported,[12] a diffraction signal from dried slime fibers was challenging to acquire due to their small diameter; however, with extended integration times on washed fibers, it was possible to observe a diffraction pattern nearly identical to that observed in the droplet and crude slime. Since previous investigations revealed that the fibrous core is comprised

DOI: 10.1021/acsnano.9b00857
ACS Nano 2019, 13, 4992−5001

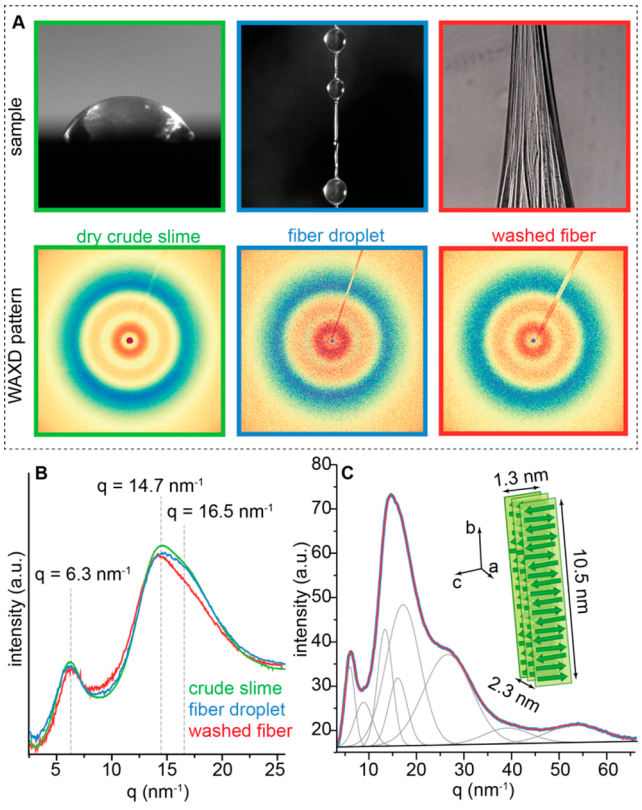

Figure 2. WAXD analysis of velvet worm slime, droplets and fibers. (A) WAXD patterns from crude slime, fiber droplets, and washed fibers are highly similar, consisting of two concentric rings. (B) Full azimuthal integration of the patterns in (A) showing intensity *vs* scattering vector *q*. (C) Peak fitting of the extended WAXD intensity *vs* *q* plot acquired from a fiber droplet with a linear background correction. Peak widths were used to estimate dimensions of *β*-crystallites as indicated in the illustration.

almost entirely of protein,[5] we conclude that this diffraction signal arises from periodic structures in the fiber proteins on the size scale of 0.1−2.0 nm.

Based on the peak maxima of the rings in the integrated radial intensity profiles from slime, droplets, and fibers (q = 6.0 nm^{-1} and 16.1 nm^{-1}; Figure 2B), these patterns are highly reminiscent of randomly oriented *β*-sheet crystallites as observed in reconstituted *Bombyx mori* silk[16,17] and squid sucker rings,[18,19] as well as films and scaffolds comprised of silk fibroin or amyloid fibers.[20,21] *β*-Sheet crystallites across an enormous range of biological and synthetic systems have a well-conserved unit cell (Figure 2C), which is defined by the interstrand hydrogen-bonding distance along the *b*-axis (∼0.94 nm) and the rise per residue (*i.e.*, translational distance between amino acids) in the *β* strand along the *c*-axis (∼0.70 nm).[22,23] The intersheet spacing along the *a*-axis is sequence dependent, influenced by the size of and interaction between the amino side chains projecting from the faces of the *β*-sheets and thus varies somewhat between different *β*-crystalline proteins in the range of about 0.5−1.0 nm.[23,24] Characteristic reflections corresponding to interplane spacings in the unit cell typically appear as well-defined spots in silk fibers, in which *β*-crystallites are preferentially oriented with respect to the fiber axis.[22−24] However, the random orientation of *β*-crystallites in squid sucker rings,[18,19] and presumably velvet worm slime and fibers, resembles patterns from polycrystalline diffraction experiments, in which distinct reflections are amalgamated into broad rings.

In this light, a closer look at an extended radial profile of the droplet (Figure 2C) reveals that the intense broad peak possesses a maximum at 14.7 nm^{-1} and a shoulder at 16.5 nm^{-1}, which have been assigned previously to overlap of the (020) and (120) reflections and the (002) peak, respectively.[16,18] Often, in *β*-crystallite WAXD patterns, the lowest observed q reflection arises from the intersheet spacing and thus determines the lattice parameter of the unit cell *a*-axis, which in velvet worm *β*-crystallites is at q = 6.01 nm^{-1}. This corresponds to a *d*-spacing of 1.05 nm, which is typical for many amyloid *β*-crystallites and assigned as the (100) reflection.[20,25] Based on these observations, we predict an orthorhombic unit cell with parameters a = 1.05 nm, b = 0.94 nm, and c = 0.70 nm, allowing calculation of predicted q positions for other expected diffraction peaks. Along these lines, broader peaks appearing at q = 26.6 nm^{-1} and 53.4 nm^{-1} are consistent with an overlap of the (040) and (003) reflections and the (080) reflection, respectively, further supporting the presence of *β*-crystalline protein structure (Figure 2C). However, as in other systems, such as the squid sucker ring, the diffraction peaks are assumed to sit on top of a broad amorphous halo representing diffuse scattering from nearest-neighbor chains of random coil protein chains.[18,22]

Based on these initial assignments, we deconvoluted the complex intensity profile of the extended droplet diffraction pattern *via* Gaussian fitting (Figure 2C, Table 1). Fitted peaks

Table 1. Peak Fitting of WAXD Profile from Fiber Droplet

q (nm^{-1})	d (nm)	width (nm^{-1})	assignment
6.013	1.045	2.467	(100)
8.894	0.706	4.387	(001)
13.400	0.469	3.688	(020) + (120)
16.100	0.390	4.553	(002)
17.197	0.365	8.361	amorphous
26.593	0.236	11.946	(003) + (040)
39.106	0.161	11.435	(060)
53.504	0.117	13.628	(080)

are consistent with reflections observed in other *β*-crystalline materials (*e.g.*, silks, amyloid fibers),[16,18] confirming our initial assumptions. Additionally, the width of the fitted peaks provides information about the dimensions of the *β*-crystallites. Scherrer analysis of the (100) reflection and the (001) and (002) peaks suggests crystallite dimensions along the *a*- and *c*-axes of 2.4 and 1.3 nm, respectively (Figure 2C). The widths of the (020/120) reflection and the higher order (060) and (080) reflections exhibit a progressive broadening (*i.e.*, width increases with increasing q), indicating internal strain in the crystallites along the *b*-axis. Plotting width *vs* q and fitting with a linear regression provides information about both the size of the crystallite and the degree of variation in the spacing, based on Williamson−Hall analysis.[26] From the regression curve, we extract a dimension of 10.5 nm along the *b*-axis of the *β*-crystallite, corresponding to about 20 *β*-strands, which is quite large, but is consistent with the *β*-crystallite dimensions proposed for lacewing eggstalk silk fibers.[27] It should be noted that this is a minimum value since the (020) reflection is likely overlapped with the (120) reflection, possibly leading to overestimation of the peak width. Based on the slope of the regression, the average distance between the strands appears to

DOI: 10.1021/acsnano.9b00857
ACS Nano 2019, 13, 4992−5001

vary by up to 25%, which may reflect an increased flexibility of the β-crystallite due to its large size. Indeed, computer simulations predict that in materials such as spider silk, smaller, nanoconfined β-crystallites are more mechanically stable under shear forces than larger high-aspect ratio β-crystallites.[28] The absence of a clear (040) peak was perplexing given the observed (020), (060), and (080) reflections; however, as already mentioned, it seems quite plausible that the broad peak fitted at q = 26.6 nm^{-1} contains contributions of both the (040) and (003) reflections, which based on calculation of the unit cell should appear at 26.74 nm^{-1} and 26.93 nm^{-1}, respectively. However, due to their strong overlap, further deconvolution would likely not reflect the actual dimensions.

FTIR Investigation of Crude Slime and Fibers Shows Conformational Transition. To verify the protein structural assignments determined from WAXD, FTIR spectroscopy was performed on wet slime, dried slime, and dried washed fibers, similar to the samples measured with WAXD. Previously, only a very small region of the full FTIR spectra of slime fibers from *E. rowelli* in the area of the amide I band was reported.[12] Here, we report a more comprehensive study of the attenuated total reflection FTIR (ATR-FTIR) spectra of wet and dried crude slime as well as transmission FTIR measurements on dried fibers. ATR-FTIR is commonly used to probe surface properties (within ~2 μm of the ATR crystal), whereas transmission FTIR probes bulk properties of materials. However, based on a previously observed tendency of the slime nanodroplets (Ø ~ 70 nm) to spread over and adhere to surfaces,[4,5] it can be stated that the ATR-FTIR signals correspond to the bulk spectra of the wet and dried slime.

When initially placed on the ATR crystal, the slime showed a weak protein spectrum dominated by water peaks (Figure 3A). Over time, peaks corresponding to protein backbone vibrations became more intense relative to the water peaks likely due to the combined effect of the gradual evaporation of water in the slime and the settling and spreading of nanoglobules on the surface of the ATR crystal, since the slime was still hydrated based on visual inspection and the presence of a strong water peak at ~2100 and 3300 cm^{-1}. During dehydration of the slime on the ATR crystal, there was a continuous drop in the intensity of water-dependent peaks, while the relative intensity of the amide II band compared to the overlapped amide I/water peaks increased. This indicates that the slime is fully dehydrated after around 20 min and that the remaining peaks arise fully from the biomolecules comprising the slime. Notably, the positions of the amide I band and amide III band, which are used to assign protein conformational structure,[29−31] shift only slightly between wet and dry crude slime, indicating that the drying process alone does not affect protein secondary structure in any appreciable way.

Transmission FTIR measurements of washed slime fibers showed similar peaks to that of wet and dried slime, confirming a dominant protein composition; however, distinct changes in the protein conformation occurring during fiber drawing are indicated by the clear shift in the amide I band maximum, which is echoed in the amide III band (Figure 3B,C). The amide I region is a complex band largely corresponding to vibrations of the C═O group of the protein backbone, and specific information about protein backbone conformation can be extracted from its shape.[31] As is customary, negative second derivative analysis of the spectra from slime and fibers was performed to highlight the component peaks of the complex

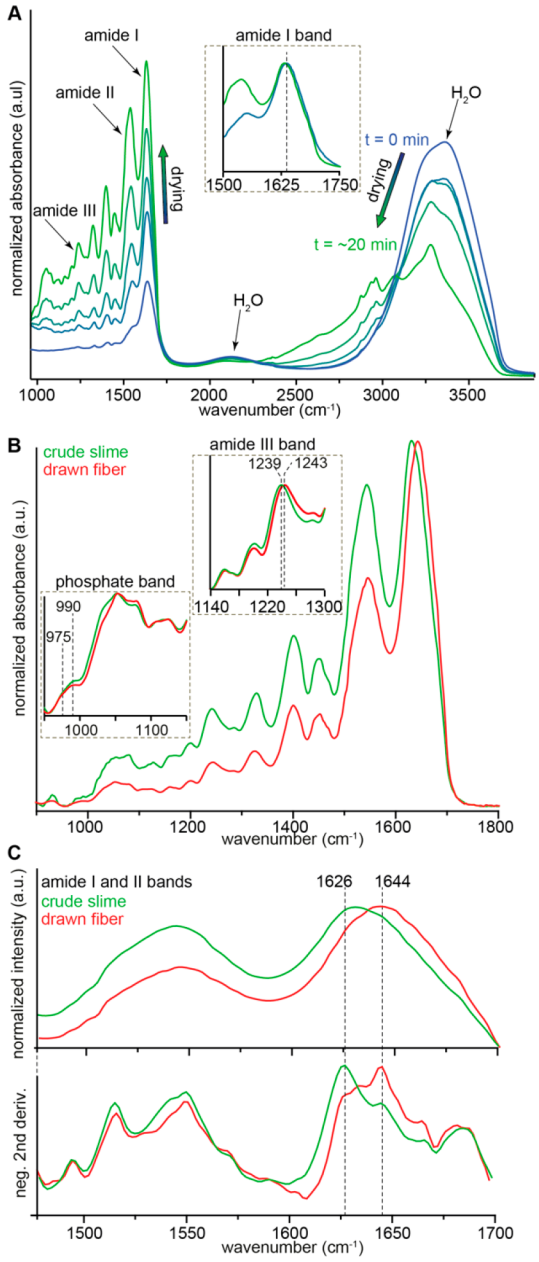

Figure 3. FTIR spectroscopy of crude slime and fibers. (A) ATR-FTIR spectra showing a time series collected from crude slime after placement on the ATR crystal and during drying over a period of ~20 min. The blue trace indicates fully hydrated slime (t = 0 min), the green trace indicates fully dehydrated slime (t = ~20 min), and the intermediate colors represent various time points between, as indicated by the colored arrows. Over time, the peaks corresponding to water decrease in intensity, while protein peaks increase. The inset shows details of amide I band in the fully hydrated *vs* dry state, indicating little change in the peak position. (B) Comparison of spectra from dried crude slime and washed fibers. Insets highlight details of the amide III and phosphate vibrational regions of the spectra. (C) Details of the amide I and II bands from (B) including negative second derivative spectra.

band,[31] indicating the presence of β-sheets (1626 cm^{-1}), β-turns (1670 cm^{-1}; 1684 cm^{-1}), and random coil structure (1649 cm^{-1}). Further support for β-sheet assignment is provided by the position of the amide III band at 1239 cm^{-1}, which appears in hydrated and dried slime at the same position, but is shifted to 1243 cm^{-1} in drawn fibers.[29,30] These

DOI: 10.1021/acsnano.9b00857
ACS Nano 2019, 13, 4992−5001

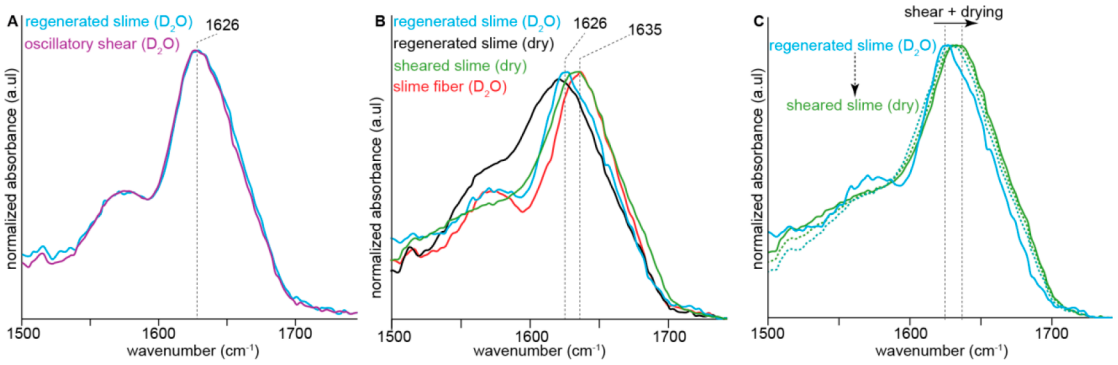

Figure 4. ATR-FTIR spectroscopy and *in situ* rheology on D_2O regenerated slime. (A) Regenerated slime in D_2O exhibits an amide I band indicating β-sheet structure, which is not significantly changed during oscillatory shear with a rheometer. (B) Intensive manual shearing of the slime on the ATR crystal performed by first compressing and then shearing and drying results in a shift of the amide I peak to higher wavenumbers, which is consistent with the shift observed in fibers formed from regenerated slime measured in D_2O. Simply drying the slime results in a slight shift in the opposite direction. (C) Measurements performed *in situ* during shearing and drying reveal a progressive transition in the position of the amide I band.

data are consistent with WAXD analysis in that they advocate for a protein structure of β-crystallites mixed with unstructured conformation, similar to a semicrystalline polymer structure. However, these data also indicate a moderate but significant loss of β-sheet structure during fiber drawing that is compensated by an increase in unstructured protein. This is consistent with predictions based on computer simulations that larger, high aspect ratio β-crystallites, as predicted for velvet worm slime proteins, will be softer and more prone to unfolding under shear forces compared with the nanoconfined β-crystallites observed in spider silk.[28]

Due to the previous report showing that the fiber-forming proteins are phosphorylated,[4] we examined the spectral range from 900 to 1150 cm^{-1}, which contains numerous well-characterized phosphate vibrations (Figure 3B). Many peaks were observed in this region, which can be tentatively assigned to various vibrations of P−O bonds of phosphate groups.[32] In particular, a small band in the region of 950−1000 cm^{-1} was previously assigned to the symmetric stretching mode of phosphates[32] and was shown to be sensitive to interaction with divalent cations.[33] Notably, in crude slime and fibers, this band consists of apparent maxima at 975 and 990 cm^{-1}, respectively. According to previous investigations on caddisfly larvae silk,[33,34] which is comprised of phosphorylated β-crystalline proteins, these two positions may represent the uncomplexed/Na^+ complexed (975 cm^{-1}) and Ca^{2+} complexed (990 cm^{-1}) forms of phosphate. This experimental finding is consistent with a previous hypothesis that transient ionic bonding mediated by divalent cations may play a critical role in both slime nanoglobular stability and fiber formation.[4]

FTIR Investigation of Reconstituted Slime with *in Situ* Rheological Analysis. In order to monitor conformational transitions occurring during shearing and fiber formation in the slime, we performed ATR-FTIR measurements during *in situ* rheological tests, which must be performed in the hydrated state. To avoid interference from the water peak with the amide I band (Figure 3A), rheological measurements were performed under N_2 flow using regenerated slime resulting from dissolving dried slime in deuterated water (D_2O). While this is not a native slime, it was previously shown that proteins in the reconstituted slime will reorganize into monodisperse nanodroplets.[5] Notably, we observe an amide I band centered at 1625 cm^{-1}, which in deuterated proteins also indicates β-sheet structure (Figure 4A).[31] This is consistent with our assignment in wet and dried slime and confirms that residual water did not interfere with the interpretation and assignment of the wet slime spectra. Shear-induced fibers formed from the D_2O-regenerated slime exhibit a significant shift in the amide I peak position to 1635 cm^{-1}, consistent with measurements on native fibers and indicating a partial loss of β-sheet structure (Figure 4B,C). Application of oscillatory shear (1% strain) with a rheometer exhibited an increase in storage modulus from 0.07 ± 0.05 kPa to 355 ± 181 kPa (n = 3), indicative of gelation, but did not result in a notable shift in the position of the amide I band peak (Figure 4A). However, manual application of a large compressive force followed by pulling and then shearing resulted in a clear shift of the amide I peak to lower wavenumbers similar to that observed in dried fibers (Figure 4B,C). Notably, we observed a progressive shift in the amide I band *in situ* over time while the shear was being applied (Figure 4C). Although the slime dries simultaneously during the intensive shear process (as occurs during natural fiber formation), simply drying the D_2O-regenerated slime results in a slight shift to lower wavenumbers (Figure 4B), clearly indicating that the shift to higher wavenumbers observed during shearing is mechanically induced. Thus, this shift, which indicates a loss of β-sheet structure in favor of a more random coil structure, represents a key step in the fiber formation process.

Polarized Confocal Raman Spectroscopy. While traditional Raman spectroscopy provides complementary data on protein conformation to confirm assignments in FTIR spectroscopy, polarized Raman spectroscopy utilizes a linearly polarized laser beam and polarized filters to probe the orientation of molecules within a material.[35] By orienting the laser polarization either parallel (Z) or perpendicular (X) to the washed fiber axis, it is possible to determine whether protein chains are oriented preferentially along a particular axis, based on intensity changes of the amide I band, as previously demonstrated in spider silk[36] and tendons.[37] Raman measurements of washed fibers reveal a sharp amide I band centered at 1671 cm^{-1} and an amide III band with a stronger peak centered at 1240 cm^{-1}, compared to the peak at 1320 cm^{-1}, both of which are consistent with the presence of extended β-sheet structure. Compared to spectra from silk,[36] however, the β-sheet content is clearly lower and likely mixed

DOI: 10.1021/acsnano.9b00857
ACS Nano 2019, 13, 4992−5001

with unstructured conformation, consistent with our FTIR and WAXD findings (Figure 5). Polarized Raman measurements of

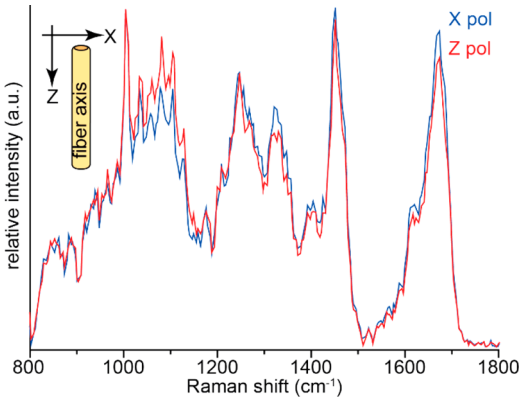

Figure 5. Polarized confocal Raman spectroscopy of washed slime fiber. Average Raman spectra acquired from washed slime fibers with laser polarization oriented parallel (Z) and perpendicular (X) to the fiber axis. Spectra are normalized to the Phe peak at 1003 cm^{-1}.

the washed velvet worm fibers indicate only a very small degree of backbone orientation with β-strands preferentially oriented along the fiber axis, based on the fact that the intensity of the amide I band in the X-polarization is marginally higher when normalized to the Phe peak (1003 cm^{-1}). However, the degree of orientation is almost negligible compared with that of silk, for example.[36] While most silks have β-crystallites oriented along the fiber axis (a notable exception being the cross-β structure observed in lacewing eggstalk silks),[27] the presence of fibrils with randomly oriented β-crystallites is observed in squid sucker rings.[19]

From β-Crystallites to Fibers: A Shear-Induced Mechanism. The ease with which many organisms rapidly process high-performance biopolymeric fibers is enviable, considering the global efforts to make polymer processing greener and more sustainable.[11,38] The velvet worm *E. rowelli*, in particular, has evolved the ability to instantly produce polymer fibers from a fluid emulsion of condensed protein-based spherical nanodroplets through simple mechanical shearing.[4,5] Velvet worms stand out compared with other fiber-forming organisms (*e.g.*, mussels, spiders) because the fibers can be drawn *ex vivo* from the slime collected from the organism, whereas most other systems depend on subtle biological control over ambient conditions (*e.g.*, pH, ionic strength, redox conditions) to induce the fluid to fiber transition.[2,38] This indicates that velvet worm slime fiber formation is based squarely on fundamental polymer physics and chemistry, and elucidation of these principles should be readily transferrable to the lab bench and beyond.

The most notable finding of this study, based on a combination of WAXD and vibrational spectroscopy, is that droplet proteins possess a substantial β-crystalline structure mixed with a random coil structure and that conformational transitions accompany fiber formation. We observed that large shear forces were required both for fibrillation and protein unfolding, whereas low shear forces led to a transition to a gel-like state, but did not lead to fiber formation or conformational changes. Based on these observations, we surmise that proteins are stored within the nanodroplets as dormant, but mechanoresponsive β-crystallites consisting of at least 20 strands per sheet as well as non-crystalline regions (Figure 6). The β-crystallites resist premature aggregation under moderate shear forces (*e.g.*, as might occur in the gland during normal movements of the animal). However, larger mechanical shear forces (*e.g.*, as occur during ejection) appear to facilitate fiber assembly by disrupting the nanodroplets and partially unfolding β-crystalline structure. Relevant to this observation, computer modeling predicts that the elongated β-crystallites present in the velvet worm slime proteins will be much softer and prone to unfolding under shear forces compared with the nanoconfined β-crystallites observed in spider silk.[28] One appealing explanation for this fibrillation behavior is that protein unfolding might present binding sites that favor intermolecular rather than intramolecular interactions; however, this remains to be seen. While shear forces are also implicated in silk drawing,[2,11,39] velvet worm slime fiber formation is quite unlike silk production in which proteins are

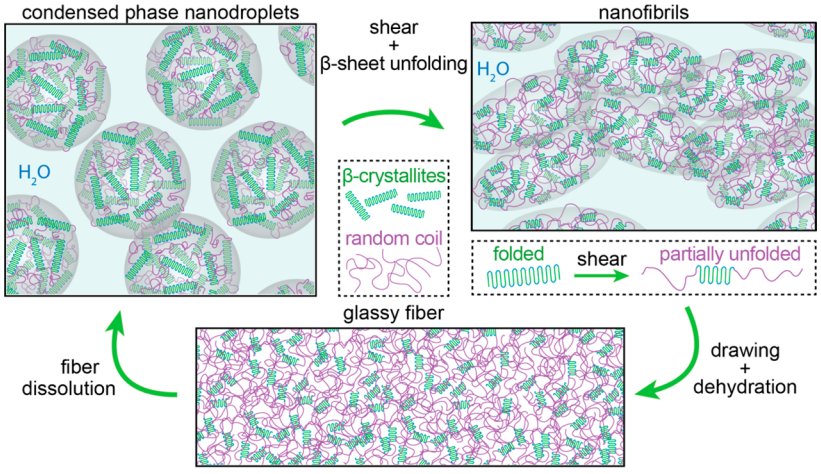

Figure 6. Schematic model of cyclic fiber processing from velvet worm slime. In the native state, *E. rowelli* slime consists of an emulsion of monodisperse nanodroplets comprised of large phosphorylated proteins with a mixture of β-crystalline and random coil structure. During mechanical shear, the droplets are perturbed, and some of the β-sheet structure is unfolded into random coil structure, which initiates aggregation of nanodroplets and fibrillation. Upon further mechanical drawing and drying, the proteins are assembled into a stiff, glassy fiber; however, dissolution of fibers in pure water leads to spontaneous reformation of monodisperse nanodroplets.

DOI: 10.1021/acsnano.9b00857
ACS Nano 2019, 13, 4992−5001

stored in a less structured conformation at high density and are converted to β-crystalline structure and aligned during drawing through subtle changes in pH, water content, and exchange of kosmotropic ions.[11]

Based on examination of the published protein sequence, it is worth pondering how the β-sheet structure forms at all, considering the high content of proline, a known helix breaker that should preclude the dihedral backbone torsion required for most regular protein folds, especially a β-sheet.[40] However, closer examination of the sequence reveals alternating patches of positively and negatively charged runs, interspersed with hydrophobic residues (Figure 1D). A more recent investigation revealed that the high molecular weight protein is phosphorylated and the slime is enriched in Ca^{2+} and Mg^{2+} ions, leading to the hypothesis that the proteins in the nanoglobules are likely stabilized by specific ionic interactions.[4] This is supported by the previously observed loss of nanoglobular structure and fiber-forming capacity when slime pH was changed and when high millimolar concentrations of NaCl were added to the slime.[4] The presence of peaks in FTIR spectra—possibly indicating phosphate-Ca^{2+}/Mg^{2+} interactions—are consistent with this hypothesis (Figure 3B). With these observations in mind, it is interesting to consider possible similarities between the slime β-crystalline structure and that of caddisfly larvae silk.[33,34] The latter is comprised of highly phosphorylated proteins that form β-crystalline structures in the presence of Ca^{2+} with the ions sandwiched between β-sheet layers.[33,34] Based on these similarities, it is conceivable that a similar mechanism may contribute to β-sheet stability in velvet worm slime proteins that would otherwise be predicted to lack structure based on the high Pro content.[12] In the case of caddisfly silk, the phosphate−Ca^{2+} interactions behave as reversible cross-links that break and reform during cyclic loading, contributing to the high toughness and self-recovery behavior.[33,34] In the case of the slime, such interactions may perform a related function, breaking during mechanical shear and reforming with neighboring molecules during fibrillation (Figure 6).

If we accept the premise that the phosphorylated proline-rich proteins are stabilized *via* non-covalent interactions in a dormant (nonassembling) state as a β-crystallite, we must then consider how mechanical agitation of the slime results in the rapid supramolecular assembly of proteins into polymeric fibers. A previous study has shown that at the nanoscale, mechanical agitation of the slime causes the droplets to coalesce, with the proteins aggregating into nano- and microscale fibrils to form the fibrous core.[5] When again exposed to water, fibers revert back to the phase-separated liquid nanodroplet state (Figure 6). This indicates that nanodroplets represent the thermodynamically stable phase of the protein, which when partially unfolded *via* mechanical shear, naturally tend to self-aggregate into fibers. Fibers, in turn, represent a metastable solid state that can be kinetically trapped *via* drying, reminiscent of protein bioglasses formed during desiccation in anhydrobiotic organisms.[31] Mechanically driven protein aggregation is observed in other systems based on shear-induced protein unfolding and the presentation of internal non-polar sites,[41−43] and mechanical shear has been also harnessed to induce formation or alter properties of protein aggregates[44] and peptide-based hydrogels.[45] It is conceivable that a similar mechanism might be at play here; however, this remains to be seen. In any case, the circular fluid to fiber transition exhibited by onychophoran slime reveals an inherent dynamicity in both the proteins and the higher order supramolecular phases, consistent with the hypothesis that stability in both nanodroplet and fiber phases of velvet worm slime is mediated *via* non-covalent charge−charge interactions.[4] As previously suggested,[4,5] the loss of water due to rapid dehydration would enable an increased strength of electrostatic interactions due to the absence of the polar solvent. This may also help to explain the circular processing, which is highly water dependent.

In light of previous investigations,[4,5] our current findings further support the hypothesis that the spherical protein nanodroplets represent a condensed liquid protein phase separation based on charge balance (*e.g.*, an internal complex coacervate), which would not be unprecedented in the realm of biological adhesives[46,47] or in the formation of biofibers.[48] However, the finding that proteins are not intrinsically disordered in this phase, but rather are partially organized into β-crystallites has not been previously observed as far as we are aware, although protein-based intracellular phase-separated liquid droplets have been implicated in the formation of β-crystalline amyloid plaques.[49] Indeed, the metastability and reversible fibrillation of the nanodroplets has many characteristics of liquid phase condensed droplets, as observed in recent studies of cellular subcompartmentalization.[49] While determining whether slime nanodroplets are actually a liquid is challenging due to the very small size, they possess several hallmarks of a condensed liquid phase: They are spherical, they coalesce and fuse, and they show a dynamicity in shape and size that is dependent on ionic strength and pH.[4,5,49,50] The possibility that the nanodroplets are a coacervate with a propensity to form viscoelastic gels that transition to a glassy solid also have a clear relevance for understanding the role of condensed liquid phases in intracellular subcompartmentalization and organization. Notably, intracellular coacervates are also metastable, exchanging cargo with the surrounding fluid phase and reversibly transitioning to glassy solid phases under certain conditions in an aggregation process known as jamming, which is a consequence of the high protein concentration.[49] While typically thought of as pathological, the tendency of protein coacervates to organize into solid phases was recently exploited in bioengineered recombinant triblock silk fusion proteins that formed self-coacervates and could be drawn into solid fibers *via* mechanical drawing.[48] These examples, together with our findings, suggest a common physicochemical underpinning, further blurring the line between pathological and functional coacervates.

CONCLUSION

In the present study, we have gained important insights into the role of protein conformation in condensed liquid nanodroplets in guiding the fiber formation in velvet worm slime. X-ray diffraction and vibrational spectroscopy provide compelling evidence that the primary phosphate-rich protein exists partially in a β-crystalline form in the slime. Previous evidence indicates that these proteins are contained within liquid phase condensed nanodroplets that are highly charge stabilized and suggests that the β-crystalline proteins may form a phase-separated coacervate spontaneously. Fiber formation occurs when nanodroplets are mechanically disrupted, leading to a concomitant change in protein conformation, triggering aggregation of proteins into fibers. Fibers apparently transition from a gel-like viscoelastic phase to a glassy phase *via* water loss, possibly through molecular jamming as the dielectric

DOI: 10.1021/acsnano.9b00857
ACS Nano 2019, 13, 4992−5001

medium changes. When water is reintroduced to the system, this process is reversed, leading to the dissolution of fibers, followed by the demixing of proteins into condensed nanodroplets, which can be reformed into fibers upon further mechanical agitation. These design principles are firmly based on fundamental physicochemical principles and, if distilled and translated properly at the lab bench, could be a potential route for circular processing of sustainable reversible polymers of the future.

EXPERIMENTAL SECTION

Sample Collection and Preparation. Experiments were performed on the peripatopsid species *Euperipatoides rowelli* Reid, 1996. Specimens of *E. rowelli* were obtained from decaying wood at the corresponding localities and maintained in the laboratory as described previously.[8] The animals were collected and exported under the following permit numbers: SL101720/2016, issued by NSW National Parks & Wildlife Service (Australia), and PWS2016-AU-001023, issued by Department of Sustainability, Environment, Water, Population, and Communities (Australia). All animal treatments complied with the principles of laboratory animal care and the German law on the protection of animals. Slime samples for each experiment were obtained from several specimens by stimulating them to eject the slime into Eppendorf tubes. Collected slime was stored in the fridge for no longer than 3−4 days at 4 °C to avoid bacterial growth or potential protein degradation. Deuterated samples for FTIR-rheometry were prepared by drying of 200 μL of slime, which was treated before with NaN_3 (0.05%) in order to avoid bacterial growth. The 20 mg of dried material was resuspended in 200 μL of D_2O under an argon-saturated atmosphere by shaking overnight at room temperature in an orbital thermoshaker (Biosan TS-100) at 300 rpm. The slime was then allowed to relax for 1 h at 30 °C without shaking prior to the analyses.

Synchrotron Wide-Angle X-ray Diffraction (WAXD). The WAXD experiments were carried out on the μSpot beamline at the synchrotron source Bessy II (Helmholtz-Center Berlin für Materialien and Energie (HZB) Berlin, Germany), with an X-ray wavelength of either 0.68880 or 0.82656 Å and a spot size of a diameter between 30 and 100 μm depending on the measurement. A 2D CCD detector (MarMosaic 225, Mar USA, Evanston, USA) with a pixel size of 73.24 × 73.24 μm^2 and a resolution of 3072 pixels × 3072 pixels was used to acquire the image frames. The measurement time per frame was 60 s for the crude slime and crude fiber droplet, respectively, and 120 s for the washed fiber. Samples were mounted on aluminum frames using the natural adhesive properties of the slime and fibers. Specifically, for the dried slime measurements, the crude slime was dried directly in the frame. To form crude fibers, a small droplet of the slime was placed on the bottom edge of the frame, and the fiber was manually drawn and adhered on the opposite edge of the frame. Measurements were made either directly in the center of the fiber or in a large droplet along the fiber. For washed fiber samples, crude fibers were placed in distilled water for several minutes, as described previously,[5] and adhered onto the frame with cyanoacrylate glue. All samples were measured in the dry state. Calibrations were carried out for each new measurement with a quartz standard to determine the sample to detector distance calculated for a given measurement using the DPDAK software.[51] The sample to detector distance was ∼16.2 cm for the crude fiber droplet, ∼ 34.2 cm for the crude slime, and ∼31.5 cm for the washed fiber. DPDAK was also used for initial data analysis (*e.g.*, background correction and azimuthal integration). Following a linear background subtraction, OPUS software (Bruker) was used to perform the fitting of azimuthally integrated 1D intensity profiles with a series of overlapping Gaussian peaks in order to estimate peak position and fwhm as previously performed on materials comprised of randomly oriented β-crystallites.[18]

To determine the crystallite size from peak width, Scherrer analysis was utilized with the following equation:

$$D_{hkl} = \frac{K\lambda}{\beta \cos \theta_\beta}$$

where D_{hkl} is the thickness of the crystallite perpendicular to plane *hkl*, λ is the wavelength of the incident X-ray beam, K is a shape-dependent constant close to unity (here, we use 0.91), β is the full-width half-maximum (fwhm) of the peak, and θ_β is the diffraction angle of the *hkl* reflection. The Williamson−Hall analysis was used to estimate crystallite size from the (020), (060), and (080) because they exhibited an increasing fwhm with an increasing q value.[26]

Fourier Transform Infrared (FTIR) Spectroscopy. Attenuated total reflection Fourier transform infrared (ATR-FTIR) spectra from wet and dried slime were recorded using a Bruker Tensor spectrometer (Ettlingen, Germany) equipped with a liquid N_2-cooled mercury cadmium telluride (MCT) detector and purged with a continuous flow of N_2 gas. A BioATRCell II accessory with a silicon ATR crystal from Bruker was used as a sampling system. Crude slime was placed on the ATR cell by gently pouring from an Eppendorf tube so as not to agitate the slime. During the evaporation experiments, crude slime was evaporated on the ATR crystal over a period of ∼30 min under N_2 flow, while simultaneously recording spectra. Transmission FTIR spectra were recorded with a Bruker Hyperion FTIR microscope coupled with a Bruker Tensor spectrometer (Ettlingen, Germany). Measurements were only taken from thin regions of the fibers to avoid artifacts associated with sample overabsorbance.[52] Spectra were measured at 25 °C. For each measurement, 32 interferograms were accumulated at a spectral resolution of 4 cm^{-1}. OPUS software (Bruker) was utilized for data collection and data processing (*e.g.*, background subtraction).

ATR-FTIR Spectroscopy during *in Situ* Rheology. Rheological experiments with *in situ* FTIR spectroscopy were performed on a combined system (Haake Mars III, Thermo Fisher Scientific coupled with Nicolet iS10) with integrated data collection. The bottom plate of the rheometer has a diamond attenuated total reflectance (ATR) element allowing for *in situ* spectroscopic measurements while quasi-simultaneously performing rheological measurements. To control the relative ambient humidity (50% RH), a homemade humidity chamber was integrated in the FTIR rheometer. This allowed RH with a 1% accuracy and performing the tests at constant 22 ± 1 °C. The RH was controlled by the (de)saturation process of a flow of nitrogen gas with either water or deuterated water, which is in turn transferred into the sample chamber. Oscillatory time sweeps were performed in this setup for 30 min with an 8 mm diameter stainless steel parallel plate geometry, a shear strain γ of 1%, and a frequency of 5 Hz. A stabilization time of 5 min prior to the measurement was applied. For all the measurements, the plate-ATR crystal gap was kept at 0.3 mm. The FTIR data were collected before, during, and after every rheological measurement. For each measurement, 16 interferograms were accumulated at a spectral resolution of 4 cm^{-1}.

Polarized Confocal Raman Spectroscopy. Spectra were acquired using a Confocal Raman Microscope (Alpha300, Witec, Ulm, Germany) equipped with a piezo scanner (P-500, Physik Instrumente, Karlsruhe, Germany). A linear polarized laser (Nd:YAG laser, λ = 532 nm) was rotated to the desired polarization using a half-wave plate and was focused on the sample, and the Raman scattered light was detected by a thermoelectrically cooled CCD detector (DU401A-BV, Andor, Belfast, North Ireland) placed behind the spectrometer (UHTS 300, WITec, Ulm, Germany). Individual spectra were acquired from 30 accumulations with an integration time of 0.5 s using a 60× objective (Nikon, Düsseldorf, Germany, NA = 0.80). Spectra were measured with the polarizer oriented parallel and perpendicular to the fiber axis. At least five spectra were collected from different regions of the fiber under both conditions and averaged. The ScanCtrlSpectroscopyPlus software (Witec, Ulm, Germany) was used for the measurement setup. OPUS software (Bruker) was utilized for background subtraction and spectral averaging.

DOI: 10.1021/acsnano.9b00857
ACS Nano 2019, 13, 4992−5001

AUTHOR INFORMATION

Corresponding Author

*E-mail: matt.harrington@mcgill.ca.

ORCID

Santiago J. Garcia: 0000-0002-2211-9972
Stephan Schmidt: 0000-0002-4357-304X
Matthew J. Harrington: 0000-0003-1417-9251

Notes

The authors declare no competing financial interest.

ACKNOWLEDGMENTS

A.B., G.M., and S.S. gratefully acknowledge support from German Research Foundation (MA 4147/7-1, SCHM 2748/5-1). M.J.H. acknowledges support from the Max Planck Society and the Natural Sciences and Engineering Research Council of Canada (NSERC Discovery grant RGPIN-2018-05243). Collecting and export permits have been kindly provided by the Office of Environment & Heritage (NSW National Parks & Wildlife Service) and the Department of the Environment of Australia for the Australian species studied and by the National System of Conservation Areas (SINAC, MINAE). The authors thank D. M. Rowell, I. d. S. Oliveira, C. Martin, and I. Schumann for help with specimen collection and photography, S. Siegel and C. Li at the μSpot beamline (BESSY, Adlershof-Berlin, Germany) as well as L. Bertinetti for helpful discussion. A.B. thanks M. Schlegel for providing laboratory and office space in Leipzig.

REFERENCES

(1) Harrington, M.; Speck, O.; Speck, T.; Wagner, S.; Weinkamer, R. Biological Archetypes for Self-Healing Materials. *Adv. Polym. Sci.* **2015**, *273*, 307−344.

(2) Heidebrecht, A.; Eisoldt, L.; Diehl, J.; Schmidt, A.; Geffers, M.; Lang, G.; Scheibel, T. Biomimetic Fibers Made of Recombinant Spidroins with the Same Toughness As Natural Spider Silk. *Adv. Mater.* **2015**, *27*, 2189−2194.

(3) Lee, B. P.; Messersmith, P. B.; Israelachvili, J. N.; Waite, J. H. Mussel-Inspired Adhesives and Coatings. *Annu. Rev. Mater. Res.* **2011**, *41*, 99−132.

(4) Baer, A.; Hansch, S.; Mayer, G.; Harrington, M. J.; Schmidt, S. Reversible Supramolecular Assembly of Velvet Worm Adhesive Fibers *via* Electrostatic Interactions of Charged Phosphoproteins. *Biomacromolecules* **2018**, *19*, 4034−4043.

(5) Baer, A.; Schmidt, S.; Haensch, S.; Eder, M.; Mayer, G.; Harrington, M. J. Mechanoresponsive Lipid-Protein Nanoglobules Facilitate Reversible Fibre Formation in Velvet Worm Slime. *Nat. Commun.* **2017**, *8*, 974.

(6) Mayer, G.; Oliveira, I. S.; Baer, A.; Hammel, J. U.; Gallant, J.; Hochberg, R. Capture of Prey, Feeding, and Functional Anatomy of the Jaws in Velvet Worms (Onychophora). *Integr. Comp. Biol.* **2015**, *55*, 217−227.

(7) von Byern, J.; Müller, C.; Voigtländer, K.; Dorrer, V.; Marchetti-Deschmann, M.; Flammang, P.; Mayer, G., Examples of Bioadhesives for Defence and Predation. In *Functional Surfaces in Biology III: Diversity of the Physical Phenomena*, Gorb, S. N.; Gorb, E. V., Eds.; Springer International Publishing: Cham, 2017; pp 141−191.

(8) Baer, A.; Mayer, G. Comparative Anatomy of Slime Glands in Onychophora (Velvet Worms). *J. Morphol.* **2012**, *273*, 1079−1088.

(9) Ruhberg, H.; Storch, V. Über Wehrdrüsen und Wehrsekret von *Peripatopsis moseleyi* (Onychophora). *Zool. Anz.* **1977**, *198*, 9−19.

(10) Baer, A.; de Sena Oliveira, I.; Steinhagen, M.; Beck-Sickinger, A. G.; Mayer, G. Slime Protein Profiling: A Non-Invasive Tool for Species Identification in Onychophora (Velvet Worms). *J. Zool. System. Evol. Res.* **2014**, *52*, 265−272.

(11) Heim, M.; Keerl, D.; Scheibel, T. Spider Silk: From Soluble Protein to Extraordinary Fiber. *Angew. Chem., Int. Ed.* **2009**, *48*, 3584−3596.

(12) Haritos, V. S.; Niranjane, A.; Weisman, S.; Trueman, H. E.; Sriskantha, A.; Sutherland, T. D. Harnessing Disorder: Onychophorans Use Highly Unstructured Proteins, Not Silks, for Prey Capture. *Proc. R. Soc. London, Ser. B* **2010**, *277*, 3255−3263.

(13) Corrales-Urena, Y. R.; Sanchez, A.; Pereira, R.; Rischka, K.; Kowalik, T.; Vega-Baudrit, J. Extracellular Micro and Nanostructures Forming the Velvet Worm Solidified Adhesive Secretion. *Mater. Res. Express* **2017**, *4*, 125013.

(14) Reid, A. Review of the Peripatopsidae (Onychophora) in Australia, with Comments on Peripatopsid Relationships. *Invertebr. Syst.* **1996**, *10*, 663−936.

(15) Jerez-Jaimes, J.; Bernal-Pérez, C. Taxonomía de Onicóforos de Santander, Colombia y Termogravimetría, Calorimetría de Barrido Diferencial y Espectroscopia Infrarroja de la Secreción Adhesiva (Onychophora: Peripatidae). *Rev. Biol. Trop.* **2009**, *57*, 567−588.

(16) Martel, A.; Burghammer, M.; Davies, R. J.; Di Cola, E.; Vendrely, C.; Riekel, C. Silk Fiber Assembly Studied by Synchrotron Radiation SAXS/WAXS and Raman Spectroscopy. *J. Am. Chem. Soc.* **2008**, *130*, 17070−17074.

(17) Gong, Z. G.; Huang, L.; Yang, Y. H.; Chen, X.; Shao, Z. Z. Two Distinct Beta-Sheet Fibrils from Silk Protein. *Chem. Commun.* **2009**, *48*, 7506−7508.

(18) Guerette, P. A.; Hoon, S.; Ding, D. W.; Amini, S.; Masic, A.; Ravi, V.; Venkatesh, B.; Weaver, J. C.; Miserez, A. Nanoconfined Beta-Sheets Mechanically Reinforce the Supra-Biomolecular Network of Robust Squid Sucker Ring Teeth. *ACS Nano* **2014**, *8*, 7170−7179.

(19) Latza, V.; Guerette, P. A.; Ding, D. W.; Amini, S.; Kumar, A.; Schmidt, I.; Keating, S.; Oxman, N.; Weaver, J. C.; Fratzl, P.; Miserez, A.; Masic, A. Multi-Scale Thermal Stability of a Hard Thermoplastic Protein-Based Material. *Nat. Commun.* **2015**, *6*, 8313.

(20) Ling, S. J.; Li, C. X.; Adamcik, J.; Shao, Z. Z.; Chen, X.; Mezzenga, R. Modulating Materials by Orthogonally Oriented Beta-Strands: Composites of Amyloid and Silk Fibroin Fibrils. *Adv. Mater.* **2014**, *26*, 4569−4574.

(21) Nazarov, R.; Jin, H. J.; Kaplan, D. L. Porous 3-D Scaffolds from Regenerated Silk Fibroin. *Biomacromolecules* **2004**, *5*, 718−726.

(22) Sampath, S.; Isdebski, T.; Jenkins, J. E.; Ayon, J. V.; Henning, R. W.; Orgel, J.; Antipoa, O.; Yarger, J. L. X-Ray Diffraction Study of Nanocrystalline and Amorphous Structure Within Major and Minor Ampullate Dragline Spider Silks. *Soft Matter* **2012**, *8*, 6713−6722.

(23) Warwicker, J. O. Comparative Studies of Fibroins 2. Crystal Structures of Various Fibroins. *J. Mol. Biol.* **1960**, *2*, 350−362.

(24) Madurga, R.; Blackledge, T. A.; Perea, B.; Plaza, G. R.; Riekel, C.; Burghammer, M.; Elices, M.; Guinea, G.; Perez-Rigueiro, J. Persistence and Variation in Microstructural Design During the Evolution of Spider Silk. *Sci. Rep.* **2015**, *5*, 14820.

(25) Jahn, T. R.; Makin, O. S.; Morris, K. L.; Marshall, K. E.; Tian, P.; Sikorski, P.; Serpell, L. C. The Common Architecture of Cross-Beta Amyloid. *J. Mol. Biol.* **2010**, *395*, 717−727.

(26) Williamson, G. K.; Hall, W. H. X-Ray Line Broadening from Filed Aluminium and Wolfram. *Acta Metall.* **1953**, *1*, 22−31.

(27) Weisman, S.; Okada, S.; Mudie, S. T.; Huson, M. G.; Trueman, H. E.; Sriskantha, A.; Haritos, V. S.; Sutherland, T. D. Fifty Years Later: The Sequence, Structure and Function of Lacewing Cross-Beta Silk. *J. Struct. Biol.* **2009**, *168*, 467−475.

(28) Keten, S.; Xu, Z.; Ihle, B.; Buehler, M. J. Nanoconfinement Controls Stiffness, Strength and Mechanical Toughness of Beta-Sheet Crystals in Silk. *Nat. Mater.* **2010**, *9*, 359−367.

(29) Ding, D. W.; Pan, J.; Lim, S. H.; Amini, S.; Kang, L. F.; Miserez, A. Squid Suckerin Microneedle Arrays for Tunable Drug Release. *J. Mater. Chem. B* **2017**, *5*, 8467−8478.

(30) Guerette, P. A.; Hoon, S.; Seow, Y.; Raida, M.; Masic, A.; Wong, F. T.; Ho, V. H. B.; Kong, K. W.; Demirel, M. C.; Pena-Francesch, A.; Amini, S.; Tay, G. Z.; Ding, D.; Miserez, A. Accelerating the Design of Biomimetic Materials by Integrating

DOI: 10.1021/acsnano.9b00857
ACS Nano 2019, 13, 4992−5001

RNA-Seq with Proteomics and Materials Science. *Nat. Biotechnol.* **2013**, *31*, 908−915.
(31) Yang, H. Y.; Yang, S. N.; Kong, J. L.; Dong, A. C.; Yu, S. N. Obtaining Information about Protein Secondary Structures in Aqueous Solution Using Fourier Transform IR Spectroscopy. *Nat. Protoc.* **2015**, *10*, 382−396.
(32) Movasaghi, Z.; Rehman, S.; Rehman, I. U. Fourier Transform Infrared (FTIR) Spectroscopy of Biological Tissues. *Appl. Spectrosc. Rev.* **2008**, *43*, 134−179.
(33) Ashton, N. N.; Stewart, R. J. Self-Recovering Caddisfly Silk: Energy Dissipating, Ca^{2+}-Dependent, Double Dynamic Network Fibers. *Soft Matter* **2015**, *11*, 1667−1676.
(34) Ashton, N. N.; Pan, H. Z.; Stewart, R. J. Connecting Caddisworm Silk Structure and Mechanical Properties: Combined Infrared Spectroscopy and Mechanical Analysis. *Open Biol.* **2016**, *6*, 160067.
(35) Galvis, L.; Dunlop, J. W. C.; Duda, G.; Fratzl, P.; Masic, A. Polarized Raman Anisotropic Response of Collagen in Tendon: Towards 3D Orientation Mapping of Collagen in Tissues. *PLoS One* **2013**, *8*, No. e63518.
(36) Lefevre, T.; Rousseau, M. E.; Pezolet, M. Protein Secondary Structure and Orientation in Silk as Revealed by Raman Spectromicroscopy. *Biophys. J.* **2007**, *92*, 2885−2895.
(37) Masic, A.; Bertinetti, L.; Schuetz, R.; Galvis, L.; Timofeeva, N.; Dunlop, J. W. C.; Seto, J.; Hartmann, M. A.; Fratzl, P. Observations of Multiscale, Stress-Induced Changes of Collagen Orientation in Tendon by Polarized Raman Spectroscopy. *Biomacromolecules* **2011**, *12*, 3989−3996.
(38) Priemel, T.; Degtyar, E.; Dean, M. N.; Harrington, M. J. Rapid Self-Assembly of Complex Biomolecular Architectures During Mussel Byssus Bio-Fabrication. *Nat. Commun.* **2017**, *8*, 14539.
(39) Heim, M.; Romer, L.; Scheibel, T. Hierarchical Structures Made of Proteins. The Complex Architecture of Spider Webs and Their Constituent Silk Proteins. *Chem. Soc. Rev.* **2010**, *39*, 156−164.
(40) Creighton, T. E. *Proteins: Structures and Molecular Properties*, 2nd ed.; W. H. Freeman: New York, 1992.
(41) Oates, K. M. N.; Krause, W. E.; Jones, R. L.; Colby, R. H. Rheopexy of Synovial Fluid and Protein Aggregation. *J. R. Soc., Interface* **2006**, *3*, 167−174.
(42) Savage, B.; Sixma, J. J.; Ruggeri, Z. M. Functional Self-Association of von Willebrand Factor During Platelet Adhesion under Flow. *Proc. Natl. Acad. Sci. U. S. A.* **2002**, *99*, 425−430.
(43) Schneider, S. W.; Nuschele, S.; Wixforth, A.; Gorzelanny, C.; Alexander-Katz, A.; Netz, R. R.; Schneider, M. F. Shear-Induced Unfolding Triggers Adhesion of von Willebrand Factor Fibers. *Proc. Natl. Acad. Sci. U. S. A.* **2007**, *104*, 7899−7903.
(44) Hill, E. K.; Krebs, B.; Goodall, D. G.; Howlett, G. J.; Dunstan, D. E. Shear Flow Induces Amyloid Fibril Formation. *Biomacromolecules* **2006**, *7*, 10−13.
(45) Aggeli, A.; Bell, M.; Boden, N.; Keen, J. N.; Knowles, P. F.; McLeish, T. C. B.; Pitkeathly, M.; Radford, S. E. Responsive Gels Formed by the Spontaneous Self-Assembly of Peptides into Polymeric β-Sheet Tapes. *Nature* **1997**, *386*, 259−262.
(46) Stewart, R. J.; Wang, C. S.; Shao, H. Complex Coacervates As a Foundation for Synthetic Underwater Adhesives. *Adv. Colloid Interface Sci.* **2011**, *167*, 85−93.
(47) Waite, J. H. Mussel Adhesion - Essential Footwork. *J. Exp. Biol.* **2017**, *220*, 517−530.
(48) Mohammadi, P.; Aranko, A. S.; Lemetti, L.; Cenev, Z.; Zhou, Q.; Virtanen, S.; Landowski, C. P.; Penttilä, M.; Fischer, W. J.; Wagermaier, W.; Linder, M. B. Phase Transitions As Intermediate Steps in the Formation of Molecularly Engineered Protein Fibers. *Commun. Biol.* **2018**, *1*, 86.
(49) Shin, Y.; Brangwynne, C. P. Liquid Phase Condensation in Cell Physiology and Disease. *Science* **2017**, *357*, No. eaaf4382.
(50) Hyman, A. A.; Weber, C. A.; Juelicher, F., Liquid-Liquid Phase Separation in Biology. In *Annual Review of Cell and Developmental Biology*; Schekman, R., Lehmann, R., Eds., 2014; Vol. *30*, pp 39−58.
(51) Benecke, G.; Wagermaier, W.; Li, C.; Schwartzkopf, M.; Flucke, G.; Hoerth, R.; Zizak, I.; Burghammer, M.; Metwalli, E.; Müller-Buschbaum, P.; Trebbin, M.; Förster, S.; Paris, O.; Roth, S. V.; Fratzl, P. A Customizable Software for Fast Reduction and Analysis of Large X-Ray Scattering Data Sets: Spplications of the New DPDAK Package to Small-Angle X-Ray Scattering and Grazing-Incidence Small-Angle X-Ray Acattering. *J. Appl. Crystallogr.* **2014**, *47*, 1797−1803.
(52) Smith, B. C. *Fundamentals of Fourier Transform Infrared Spectroscopy*, 2nd ed.; CRC Press: Boca Raton, 2011.

DOI: 10.1021/acsnano.9b00857
ACS Nano 2019, 13, 4992−5001